Polymer-free hydrogel made of lipid nanocapsules, as a local drug delivery platform

Marion Pitorre, Claire Gazaille, Le Thuy Trang Pham, Karolina Frankova, Jérôme Béjaud, Nolwenn Lautram, Jérémie Riou, Rodolphe Perrot, Franck Geneviève, Valérie Moal, et al.

Version of Record: https://www.sciencedirect.com/science/article/pii/S0928493121003271
Manuscript_373560c619fabb4a6aebe44ddac6f0e5

Polymer-free hydrogel made of lipid nanocapsules, as a local drug delivery platform.

Marion Pitorre[1], Claire Gazaille[1], Le Thuy Trang Pham[1], Karolina Frankova[1], Jérôme Béjaud[1], Nolwenn Lautram[1], Jérémie Riou[1], Rodolphe Perrot[2], Franck Geneviève[3], Valérie Moal[4], Jean-Pierre Benoit[1], and Guillaume Bastiat[1,*]

1 Univ Angers, Inserm, CNRS, MINT, *SFR* ICAT, F-49000 Angers, France.
2 Univ Angers, Service Commun d'Imageries et d'Analyses Microscopiques (SCIAM), *SFR* ICAT, F-49000 Angers, France.
3 Hematology Department, University Hospital, Angers, France.
4 Biochemistry and Molecular Biology Department, University Hospital, Angers, France.
* Corresponding author. electronic address: guillaume.bastiat@univ-angers.fr.

Abstract

Nanoparticle-loaded hydrogels are attractive pharmaceutical drug delivery systems that combine the advantages of both hydrogel (local administration and/or sustained drug release) and nanoparticle (stealthiness, targeting and decreased toxicity). The design of nanoparticle-loaded hydrogels is largely conventional, consisting of the dispersion of nanoparticles in a natural or synthetic polymer matrix to form a gel network. Novel nanoparticle-loaded hydrogels architecture could provide advantages in terms of innovation and application. We focused on the development of lipid nanocapsule (LNC)-based hydrogels without the use of a polymer matrix as a platform for drug delivery. Cytidine was modified by grafting palmitoyl chains (CytC16) and the new entity was added during the LNC phase-inversion formulation process allowing spontaneous gelation. Positioned at the oil/water interface, CytC16 acts as a crosslinking agent between LNCs. Association of the LNCs in a three-dimensional network led to the formation of polymer-free hydrogels. The viscoelastic properties of the LNC-based hydrogels depended on the LNC concentration and CytC16 loading but were not affected by the LNC size distribution. The LNC and drug-release profiles were controlled by the mechanical properties of the LNC-based hydrogels (slower release profiles correlated with higher viscoelasticity). Finally, the subcutaneous administration of LNC-based hydrogels led to classic inflammatory reactions of the foreign body-reaction type due to the endogenous character of CytC16, shown by cellular viability assays. New-generation nanoparticle-loaded hydrogels (LNC-based polymer-free

hydrogels) show promise as implants for pharmaceutical applications. Once LNC release is completed, no gel matrix remains at the injection site, minimizing the additional toxicity due to the persistence of polymeric implants. Sustained drug-release profiles can be controlled by the mechanical properties of the hydrogels and could be tailor-made, depending on the therapeutic strategy chosen.

Keywords

Lipid nanocapsule, hydrogel, sustained release, nanomedicine, modified cytidine, subcutaneous injection.

1. Introduction

Nanomedicine research is exceptionally active (large investments of time and money), with the objective of developing innovative therapeutic strategies for diseases such as cancer [1]. Nanotechnologies provide new pharmacological properties to active pharmaceutical ingredients (APIs) that depend on the nanoparticles used, thus increasing their efficiency. Advantages, such as prolonged systemic circulation, passive or active targeting, and the possibility of combining APIs, lead to better pharmacokinetic and biodistribution profiles for higher therapeutic indices [2-4]. Used initially for the treatment of cancer [1,5], nanomedicines have been developed for other diseases, such as atherosclerosis and diabetes [6,7], as well as for other medical applications, such as *in vivo* imaging and tissue engineering [8].

Nanomedicines are generally used in suspension for intravenous therapeutic strategies and are administered alone (repeated or not, depending on the administration protocol). When used in suspension, this pharmaceutical technology is of limited interest for medical applications that require local administration or the sustained release of drugs. However, hydrogel-based technologies can be used to impart the properties necessary for such applications. Hydrogels are among the oldest technologies used for pharmaceutical applications and are still the ideal system for ocular [9,10], nasal [11], vaginal [12], intestinal [13], intra-articulary [14], intracerebral [15], and skin administration [16]. Hydrogels are drug-delivery platforms of which the three-dimensional polymer network of the hydrogel provides an ideal opportunity for the sustained release of APIs, such as proteins [17]. Hydrogel-based technologies are being developed to improve their delivery by stimuli-responsive *in situ* gelation [18]. Patient compliance and observance are improved with repeated administration that is generally painless and limited. An important innovation has been the development of hybrid materials, biosynthetic structures with cell-loaded hydrogels, which show promise for tissue engineering and *in vivo* regeneration [19], as well as for *ex vivo* applications. Indeed, the hydrogel mimics the extracellular matrix and guides cell development or differentiation. Studies have also been carried out to define new applications in immunological therapies, such as vaccine development [20].

Hydrogels loaded with nanoparticles offer promising avenues for developing new therapeutic strategies, combining the advantages of both nano- and hydrogel technologies. Eleven clinical trials are currently referenced worldwide (https://clinicaltrials.gov/, accessed January 4, 2021).

They include the study of using inorganic nanoparticles, such as silver nanoparticles (antibacterial treatments), quantum dots coated with a somatostatin analog (breast cancer imaging and treatment), nanocrystals of hydroxyapatite (chronic periodontitis), nanocrystals of curcumin (oral aphthous ulcer treatment), nanoparticles encapsulating capsaicin (painful diabetic neuropathy treatment), and nanoparticles of chitosan encapsulating chlorhexidine (pulp necrosis treatment). The combination of nanotechnologies with hydrogels is increasingly being considered for medical applications. Over the past decade, promising preclinical results have been reported concerning the use of liposomes, micelles, liquid and solid lipid nanocapsules, polymer nanoparticles, dendrimers, and fullerenes. Nanoparticles loaded into a hydrogel matrix have shown promising results for medical applications, such as for the treatment of cancer, infections, skin or inflammatory diseases, anesthesia, and analgesia, to name a few examples [21].

The various recent studies using nanoparticle-loaded hydrogels apply the same formulation strategy, i.e., dispersion of the nanoparticles in a natural gel or synthetic polymer matrix, with the addition of the nanoparticles before or after gelation [21]. These studies are innovative in terms of the nature of the nanoparticles, which obviously depends on the encapsulated APIs, or their intrinsic pharmacological properties, such as fullerenes. The diseases treated by new administration routes involving nanoparticle-loaded hydrogels may also be original and of interest. However, very few studies of nanoparticle-loaded hydrogels have focused on developing strategies based on novel architectures that are different from those conventionally used. This would be a leap forward in terms of innovation, with a positive impact on the pharmacokinetic and biodistribution properties of the nanoparticles and the APIs as well incorporated into them.

Recently, lipid nanocapsule (LNC)-based hydrogels were obtained without the use of a polymer matrix. The formulation of the LNCs (oil-in-water nanoemulsions) is based on a phase inversion process and has been widely reported over the last 20 years [22-27]. Generally, the LNCs are obtained in aqueous suspension. To obtain the hydrogel form, LNCs can be linked together following the addition of modified gemcitabine (lauroyl derivatives, GemC12), with amphiphilic properties, to their surface. Gemcitabine moieties at the LNC surface interact with each other via hydrogen bonds, leading to inter-LNC associations and forming a tridimensional network, without using a polymer [23]. Such LNC-loaded hydrogels were tested by Wauthoz, *et al*, to develop a sustained-release treatment for lung-cancer metastases. The formulation was

subcutaneously administered to mice bearing orthotopic mediastinal metastases of non-small-cell lung tumor xenografts (Ma44-3 cell line, first implanted in the lung). Analysis of the biodistribution showed that the LNCs were released from the administration site and targeted the lymph nodes, particularly the mediastinal lymph nodes, without reaching the systemic circulation. This treatment significantly delayed the death of mice relative to the group of animals without gemcitabine, with a lower administration frequency and significantly lower systemic toxicity than that following intravenous administration of GemC12-loaded LNCs in suspension [24].

More recently, Bastiancich, *et al*, tested the same hydrogel formulation for local and sustained delivery of gemcitabine for the treatment of glioblastoma. They compared a GemC12-loaded LNC-based hydrogel with modified or non-modified gemcitabine in suspension after intra-tumoral administration to subcutaneous glioblastoma xenograft-bearing mice (U87-MG cell line). The drug-loaded hydrogel formulation significantly reduced tumor size, whereas the free drug did not modify tumor growth [25]. Orthotopic resection rat and mouse models were developed to closely mimic the human clinical context for the glioblastoma therapy. The GemC12-loaded LNC-based hydrogel was used as an implant to fill the resection cavity and the animals showed longer median survival than those treated with the aqueous gemcitabine suspension (deposited in the cavity). Furthermore, short-term tolerability studies (up to 6 months) showed such LNC-based hydrogels to be suitable for local treatment in the brain (healthy mice) [26,27].

We decided to develop LNC-based hydrogels without gemcitabine as a drug-delivery platform for multi-therapeutic applications to limit the inherent toxicity of this API. Thus, we synthesized an endogenous crosslinking agent using cytidine, based on previous studies with gemcitabine. Various aliphatic chain lengths were grafted onto cytidine and the modified cytidine with amphiphilic properties similar to those of GemC12 was selected. Then, this molecule (CytC16) was added during the LNC formulation process. The viscoelastic properties of the obtained LNC-based hydrogels were measured and the influence of LNC size, LNC concentration, and CytC16 concentration were determined. Then, the release of LNCs, the injectability of the hydrogels, and the toxicity of CytC16-loaded LNCs were evaluated. Finally, an *in vivo* tolerance study was performed after subcutaneous administration of the LNC-based hydrogels.

2. Materials and Methods

2.1. Synthesis of modified gemcitabine and modified cytidine

The compounds 4-(N)-lauroyl cytidine (CytC12), 4-(N)-myristoyl cytidine (CytC14), and 4-(N)-palmitoyl cytidine (CytC16) were synthesized based on previous studies with 4-(N)-lauroyl gemcitabine (GemC12) [23]. Briefly, a gemcitabine or cytidine base (1 mmol) (263 or 243 mg, respectively) (Sigma-Aldrich, France) at 50 mg/mL in water (Milli-Q plus system, Millipore, France) was added, drop by drop, to a solution of lauric anhydride, myristic anhydride, or palmitic anhydride (2 mmol) (765, 877, and 990 mg, respectively) (Sigma-Aldrich, France) at 50 mg/mL in dioxane (Sigma-Aldrich, France) at 50°C under magnetic stirring. The reaction was monitored for 48 h by thin-layer chromatography (dichloromethane/methanol 85/15 (*v/v*) (Fischer Scientific, France) at a UV wavelength of 254 nm (Lampe UV VL-6.C (6 W – 254 nm), Fisher Scientific, France)). Evaporation under vacuum was performed at 40°C to remove reaction solvents. The residue was purified by silica gel (Sigma-Aldrich, France) column flash chromatography (gradient elution with a mixture of dichloromethane/methanol from 95/5 to 85/15 (*v/v*)). Pure fractions were collected and evaporated under vacuum to obtain white products as the main product. The characterization of GemC12, CytC12, CytC14, and CytC16 were reported in Supplementary discussion - Characterization of modified gemcitabine and cytidine.

2.2. Tensiometry

Absorption kinetics were measured at the Labrafac® WL 1349 (Labrafac) (Gattefossé, France)/water interface (rinsing drop method) using a drop tensiometer device (Tracker Teclis, France). GemC12, CytC14, or CytC16 were diluted in Labrafac from 0 to 6 mg/g. Briefly, a Labrafac drop (5 µL) was formed with an Exmire microsyringe (Prolabo, France) in an optical glass bowl (Hellma, France) containing a water phase. The axial symmetric shape (Laplacian profile) of the drop was analyzed using a video camera connected to a microcomputer. The interfacial tension, surface area and volume of the drop were recorded in real time (five measurements per second) from numerical image analysis, with the Laplace equation integrating the drop profile points. The drop volume was controlled by the syringe piston movements connected to a stepping motor to maintain a constant surface area. The absorption kinetics consisted of the formation of the GemC12, CytC14, or CytC16 monolayer by the gradual

diffusion of the amphiphilic molecules from the drop's core (Labrafac) to the interface until complete saturation was achieved. Saturation was reached when the surface tension stabilized. The experiments were repeated in triplicate for each GemC12, CytC14, or CytC16 concentration.

2.3. Formulation of the LNC suspension

The LNC formulation was based on a phase-inversion process from oil-in-water emulsion at a low temperature to water-in-oil emulsion at a high temperature and has already been extensively described.[20-22]

The quantities of oil phase (Labrafac), aqueous phase (water and sodium chloride (NaCl) (Sigma-Aldrich, France)), and surfactants (Kolliphor® HS15 (Kolliphor) (BASF, Germany) and Span® 80 (Span 80) (Sigma-Aldrich, France)) for each formulation were precisely weighed: for LNCs with a 25-nm diameter: $m_{Labrafac}$ = 600 mg, $m_{Kolliphor}$ = 1800 mg, m_{Span80} = 300 mg, m_{NaCl} = 54 mg, and m_{Water} = 1300 mg; for LNCs with a 50-nm diameter: $m_{Labrafac}$ = 1116.8 mg, $m_{Kolliphor}$ = 916.8 mg, m_{Span80} = 450 mg, m_{NaCl} = 54 mg, and m_{Water} = 1516.8 mg; for LNCs with a 75-nm diameter: $m_{Labrafac}$ = 1800 mg, $m_{Kolliphor}$ = 1300 mg, m_{Span80} = 300 mg, m_{NaCl} = 54 mg, and m_{Water} = 600 mg; for LNCs with a 100-nm diameter, $m_{Labrafac}$ = 1800 mg, $m_{Kolliphor}$ = 950 mg, m_{Span80} = 300 mg, m_{NaCl} = 54 mg, and m_{Water} = 950 mg.

Mixtures were heated to 75°C under magnetic stirring followed by cooling to 45°C (rate of 5°C/min). This cycle was repeated three times and during the last temperature decrease at the phase-inversion temperature, i.e., 55°C, an irreversible shock was induced by dilution with 2 g cold water (4°C), leading to the LNC suspension. The concentration of the LNC suspensions was adjusted by dilution with pure water.

For 3,3'-dioctadecyloxacarbocyanine perchlorate (DiO) (Fisher Scientific, France)-loaded LNC suspensions, DiO was first dissolved in Labrafac at a concentration of 0.1% ($w/w_{Labrafac}$) before adding the other constituents and proceeding to the formulation process. LNC and DiO-loaded LNC suspensions were stored at 4°C.

2.4. LNC hydrogel preparation

GemC12 or CytC16 were first solubilized in a mixture of Labrafac, Span80, and acetone (Fischer Scientific, France) at a concentration of 5 and 7.5% ($w/w_{Labrafac}$) for GemC12 and 1, 2.5, and 5% ($w/w_{Labrafac}$) for CytC16. Acetone was evaporated before the addition of Kolliphor, NaCl, and water. The weights for each ingredient were the same as those for the preparation of the LNC suspensions, according to the size of the LNCs. The rest of the formulation process was the same as for the LNC formulation for the temperature cycles and the addition of cold water at the phase inversion zone during the third cooling step. The volume of added water was adjusted depending on the final concentration of the LNCs. During the cooling to room temperature, the viscosity of the LNC suspensions loaded with GemC12 or CytC16 increased progressively, leading to a hydrogel with a waxy aspect. Before the increase in viscosity, syringes were filled with the suspensions and stored at 4°C. The gelation process was considered to be achieved after 24 h at 4°C. For DiO-loaded LNC-based hydrogels or Nile Red (NR) (Sigma-Aldrich, France)-loaded LNC-based hydrogels, DiO or NR were first dissolved in Labrafac at a concentration of 0.1% ($w/w_{Labrafac}$) before proceeding to the formulation protocol. For fluorescein (Sigma-Aldrich, France) solubilized in the LNC-based hydrogel, fluorescein was first solubilized in the water added at the end of the formulation process to obtain a concentration of 0.1 mg/mL in the final LNC-based hydrogels.

2.5. Characterization of size distribution and zeta potential

The size distribution, i.e., hydrodynamic diameter (Z-ave) and polydispersity index (PdI), and zeta potential (ZP) of both LNC suspensions and LNC-based hydrogels (before the completion of gelation and after hydrogel dissolution) were measured using a Zetasizer® Nano ZS (Malvern Panalytical, United Kingdom). The quasi-elastic light scattering instrument is equipped with a 4-mW Helium–Neon laser with an output wavelength of 633 nm and a scatter angle fixed at 173°. The correlation functions were fitted using an exponential fit (Cumulant approach) for the Z-ave and PdI determinations. The Smoluchowski approximation was used to determine the electrophoretic mobility required for ZP determination. All the measurements were performed at 25°C at a LNC suspension concentration of approximately 5 mg/mL (dilution in water).

2.6. Rheological properties

The viscoelastic properties of the LNC-based hydrogels after 24 h of storage (completed gelation) or longer, with or without extrusion through various sized needles (18, 21, and 26 gauge (G), corresponding to internal diameters of the needles of 1.2, 0.8, and 0.45 mm, respectively), were measured at 25°C using a Kinexus® rheometer (Malvern Panalytical, United Kingdom) with a cone plate geometry (diameter: 40 mm, angle: 2°). Oscillatory strain sweeps at a constant frequency of 1 Hz were performed to determine the linear regime characterized by the constant dynamic moduli (elastic modulus: G' and viscous modulus: G''), independent of the strain amplitude. In this regime (0.1% constant oscillatory strain amplitude), G' and G'' were measured as a function of oscillatory frequency (from 0.1 to 100 Hz). All the experiments were repeated three times.

2.7. Confocal microscopy

DiO-loaded LNC-based hydrogels and DiO-loaded LNC suspensions were deposited on glass slides (24×36 mm) and observed by confocal microscopy on a Leica TSC SP8 AOBS (Leica Microsystems, Germany) using LAS X software. Images were captured with a HC PL APO CS2 63X/NA 1.40 oil objective and a 3X zoom. The excitation of DiO was performed with the 488 nm line of an argon ion laser (40 mW) and the fluorescence emission collected using a gateable GaAsP hybrid detector between 492 and 600 nm.

2.8. CytC16 titration

The CytC16 concentrations in the LNC-based hydrogels were determined using a LC-MS/MS apparatus: Alliance® 2695 system (Waters Corporation, United States) with a Zorbax – Eclipse XDB-C18 column (4.6×150 mm, 3.5 µm) (Agilent Technologies, United States). The temperature was fixed at 25°C. The mobile phase consisted of methanol with formic acid 0.1% (*v/v*) (Fisher Scientific, France) at a flow rate of 0.8 mL/min. The injection volume was 10 µL. The total HPLC effluent was directed into a Quattro Micro® triple quadrupole mass spectrometer (Waters Corporation, United States). Ionization was achieved using electrospray in the positive ion mode. The mass spectrometer was operated in the multiple reactions monitoring (MRM) mode. The (M - H) + m/z transitions for Cyt-C16 were 482 > 112 and 482 > 350. For the

calibration curve, CytC16 was diluted in methanol from 1.25 to 200 ng/mL in the presence of non-loaded LNCs. For the samples, LNC-based hydrogels (50 µL) were dissolved with water at 1/4000 (*v/v*) to obtain complete dispersion of the LNCs. Then, a volume of 100 µL was mixed with 900 µL methanol. Quantification of CytC16 was achieved after filtration of this solution through a 0.22-µm filter.

2.9. LNC release from hydrogel dissolution

At the end of the formulation process and prior to gelation, the NR-loaded LNC-based hydrogels or fluorescein solubilized in LNC-based hydrogels (300 µL) were carefully deposited onto the bottom of a glass hemolysis tube (right edge, round bottom, 6 mL) (NAFVSM, France). The suspensions were stored overnight at 4°C to allow completed gelation. Then, a volume of 5.7 mL artificial extracellular matrix solution (1mg/mL hyaluronic acid, 6.4 mg/mL NaCl, 0.09 mg/mL magnesium chloride hexahydrate ($MgCl_2 \cdot 6H_2O$), 0.4 mg/mL potassium chloride (KCl), 0.1 mg/mL calcium chloride ($CaCl_2$), and 2.1 mg/mL sodium hydrogenocarbonate ($NaHCO_3$) (Sigma-Aldrich, France), pH = 7.4, 37°C) was carefully added to the top of the hydrogels, without modifying their shape. The tubes were then sealed and stored in the dark at 37°C. The supernatants (200 µL) were collected at fixed time intervals and replaced with 200 µL fresh medium (at 37°C). The collected samples were placed in a 96-well plate (GmbH, Germany). The fluorescence intensities were measured with a Fluoroscan Ascent® plate reader (Labsystems SA, France), with excitation and emission wavelengths set to 515 and 590 nm for NR and 485 and 515 nm for fluorescein, respectively. The cumulative release profiles of the NR-loaded LNCs or fluorescein were obtained, considering that 100% release corresponds to the fluorescence intensity value obtained for the complete dissolution of the LNC-based hydrogels. The NR and fluorescein fluorescence intensity values are proportional to the NR (encapsulated in the LNCs) and fluorescein concentrations within the entire range of concentrations considered in the study. Thus, the fluorescence intensity of the samples was measured without further dilution.

2.10. Cell culture and cytotoxicity

The THP-1 cell line (human monocyte/macrophage cell line) (ATCC, United States) was grown in suspension at 37°C, 90% humidity, 5% CO_2 in RPMI 1640 medium (Lonza, Belgium), completed with 10% (*v/v*) decomplemented fetal bovine serum (FBS) (Lonza, Belgium), 100 UI/mL penicillin, 100 mg/mL streptomycin, 0.25 mg/mL amphotericin B, 10 mM HEPES (1% (*v/v*)), 100 mM sodium pyruvate (1% (*v/v*)), and 20 µM β-mercaptoethanol (1% (*v/v*)) (Sigma-Aldrich, France). The cells (15×10^3 cells/well in 200 µL medium) were then plated in a 96-well cell-culture dish. Cell differentiation was induced in the same medium by adding phorbol 12-myristate 13-acetate (PMA) 200 nM (Sigma-Aldrich, France) and the plates were incubated at 37°C for 48 h to allow the cells to adhere. After aspiration of the medium to eliminate non-adherent cells, the cells were washed again with fresh medium.

The B6-KPC3 cell line (pancreas tumor from transgenic KPC mice) (gift from the Department of Oncology and Surgical Sciences of Padova, Pr. Vincenzo Bronte) was grown in suspension at 37°C, 90% humidity, 5% CO_2 in DMEM medium (Lonza, Belgium), completed with 10% (*v/v*) decomplemented FBS, 100 UI/mL penicillin, 100 mg/mL streptomycin, 0.25 mg/mL amphotericin B, 10 mM HEPES (1% (*v/v*)), 2 mM L-glutamine (1% (*v/v*)), and 20 µM β-mercaptoethanol (1% (*v/v*)). The cells (3.5×10^3 cells/well in 200 µL medium) were then plated in a 96-well cell culture dish and left to grow for 48 h at 37°C.

The cytotoxicity of diluted LNCs from LNC suspensions or dissolved LNCs from LNC-based hydrogels (Z-ave = 50 or 100 nm), loaded or not with 2.5% CytC16 ($w/w_{Labrafac}$), in cell culture medium was determined. Fresh cell-culture medium was used as controls. Various amounts of LNCs (from 0.1 to 20 mg/mL) were added to the wells and incubated with the cells for 48 h. The number of living cells was determined using a 3-(4,5-dimethylthiazol-2-yl)-5-(3-carboxymethoxyphenyl)-2-(4-sulfophenyl)-2H-tetrazolium salt (MTS) assay (colorimetric assay based on the conversion of a tetrazolium salt into formazan) (Promega, United State). Formazan absorbance was measured at 492 nm and 750 nm directly from the wells using a spectrophotometer Multiscan Ascent® MP reader (Thermo Scientific, France) after exposition to MTS (20 µL per well) for 2.5 h at 37°C. The percentage cell viability was calculated according to the following equation:

$$\text{Alive cells (\%)} = \frac{\text{Abs (T)}}{\text{Abs (C)}} \times 100$$

where Abs (T) and Abs (C) are the absorbance values of cells incubated with LNCs and cells incubated with fresh medium (control), respectively. The quantity of formazan is proportional to the number of living cells in the culture.

2.11. *In vivo* biocompatibility

All the animal experiments were performed in agreement with the EEC guidelines and the "Principles of Laboratory Animal Care" (NIH Publication No. 86-23, revised 1985) and the agreement of the "Comité d'Ethique pour l'Expérimentation Animale des Pays-de-la-Loire" (authorization CEEA 2012-37 and 2012-73). Eight-week-old female Sprague-Dawley rats were raised, housed, and maintained in the Angers University animal facility (SCAHU) under controlled conditions (12-h light/dark schedule, 24°C, tap water and chow provided *ad libitum*) throughout the study. The weight, general appearance, and behavior of the rats were monitored daily.

Thirty-nine rats were randomly divided into three groups (no administration (n = 3), sesame oil (control, approved for subcutaneously and intramuscularly administered drug formulations) (n = 18) (Croda, United States), and LNC-based hydrogel (Z-ave = 50 nm, 2.5% CytC16 ($w/w_{Labrafac}$), LNC concentration 400 mg/mL) (n = 18)) and euthanized at various time points (n = 3 per time point per group). The rats received a single subcutaneous injection of the appropriate formulation (500 µL, 18-G needle) in the shaved higher dorsal area under isoflurane anesthesia (5% in oxygen at a flow rate of 3 L/min) (Isoflurane Belamont, Belamont Laboratoires, France). After administration, the needle was held in place for 10 s to prevent leakage of the implant from the injection site.

At the various time points (1-, 2-, 4-, 7-, 14-, and 28-days *post* administration), the rats were once again anesthetized under isoflurane, euthanized by cardiac puncture, and the tissues adjacent to the injection site and remaining implants (3 x 3 cm pieces) were collected and fixed with 10% neutral-buffered formalin (Sigma-Aldrich, France).

A 500-µL volume of collected blood was put into EDTA-K2 vials (Microtainer® MAP K2 EDTA) (Becton, Dickinson and Company, United States) and stored at 4°C to determine the hematological parameters. An additional 500-µL volume of collected blood was put into vials containing heparin (Li-Heparin - Tube Micro, Sarstedt, France) and centrifuged (15 min,

2000 × g, 4°C). Approximately 200 µL plasma was recovered and stored at -20°C for biochemical analysis. Hematological and biochemical profiles were characterized at the University Hospital of Angers using standard protocols. The studied parameters were: i) red blood cell (RBC) count, hemoglobin, hematocrit, mean cell volume (MCV), mean corpuscular hemoglobin (MCH), mean corpuscular hemoglobin concentration (MCHC), platelet count, mean platelet volume (MPV), and white blood cell (WBC) counts and differentials (percentage of neutrophils, lymphocytes, monocytes, eosinophils, and basophils) for hematological profiles and ii) concentrations of urea, sodium, potassium, chloride, creatinine, alkaline phosphatase, aspartate amino transferase (AST), and alanine amino transferase (ALT) for the biochemical profiles.

The tissues adjacent to the injection site were processed and embedded in paraffin. Glass slides with 5-µm tissue sections were prepared using a Leica 2155 microtome (Leica Microsystems Inc., Canada). Slides of each implant were stained according to a hematoxylin-eosin-saffron standard protocol of the University Hospital of Angers. The slides were observed using a Scanscope® CS System scanner (Aperio Technologies, Leica Biosystems Imaging, Germany) to obtain high-resolution images. The local inflammatory response was assessed by histological evaluation of the surrounding tissue for signs of acute inflammation (neutrophils and eosinophils) and chronic inflammation (histocytes, plasmocytes, lymphocytes, multinucleated giant cells, fibroblasts, neo-angiogenesis, and collagen deposition). The intensity of the response was graded on a scale from normal (0), to minimum (+/-), medium (+), moderate (++), or high (+++), depending on the number of cells and the general appearance of the tissues.

2.12. Statistical analysis

All the results were expressed as the mean ± standard deviation (SD). Statistical analysis was performed using the non-parametric Mann-Whitney or Kruskal-Wallis tests, followed by the *post-hoc* Dunn test for pairwise comparisons. Differences were considered statistically significant for $p < 0.05$.

3. Results

3.1. Amphiphilic properties of modified cytidine

A new architectural design for nanoparticle-loaded hydrogels was recently developed using lauroyl-modified gemcitabine (GemC12) (Fig. 1 for GemC12 chemical structure). Located at the surface of the LNCs, this amphiphilic molecule acts as a crosslinking agent, allowing inter-nanoparticle interactions between LNCs similar to a tridimensional pearl necklace, resulting in a LNC-based hydrogel. Only the auto-associated LNCs form the hydrogel and no polymer was used to form the hydrogel matrix, unlike for conventional nanoparticle-loaded hydrogels [23]. Such a system was successfully tested *in vivo* after subcutaneous administration in a murine model as implants to delay the appearance of mediastinal metastases during lung cancer progression [24]. It was also used to fill the resection cavity after surgery for glioblastoma and delayed glioblastoma recurrence at the periphery of the cavity [26,27].

We replaced gemcitabine (antimetabolite drug mainly used for cancer therapies) with its endogenous analog, cytidine, with the objective to develop this new concept as a drug-delivery platform for diseases other than cancer requiring the local and sustained release of APIs. Lauroyl-modified cytidine (CytC12) was synthesized and its likely location at the LNC surface assessed by investigating its amphiphilic properties at the Labrafac/water interface. However, although GemC12 is soluble in Labrafac, CytC12 is not. The hydrophilic-hydrophobic balance of CytC12 is shifted towards a more hydrophilic character than that of GemC12 due to an additional hydroxyl function on cytidine.

Thus, the synthesis of modified cytidine molecules was performed using longer aliphatic chains, and myristoyl-modified and palmitoyl-modified cytidine (CytC14 and CytC16 (Fig. 1 for CytC16 chemical structure), respectively) were obtained. These two molecules were soluble in Labrafac up to at least 0.6% (*w/w*), showing that their hydrophilic-hydrophobic balance was shifted towards a more lipophilic character than that of CytC12. Their amphiphilic properties were verified using a drop tensiometer. CytC14 and CytC16 showed amphiphilic properties, as the surface tension of the Labrafac/Water interface decreased when the concentrations of these two modified cytidines increased. The surface tension of the interface decreased by 40 ± 4% and 62 ± 6% for CytC14 and CytC16, respectively, from 0 to 0.6% ($w/w_{Labrafac}$) (Fig. 1), whereas the surface tension of the interface decreased by 60 ± 2% in the same concentration range for

GemC12. We decided to select CytC16 to develop the design of new LNC-based hydrogels due to the similar amphiphilic properties of the two modified molecules.

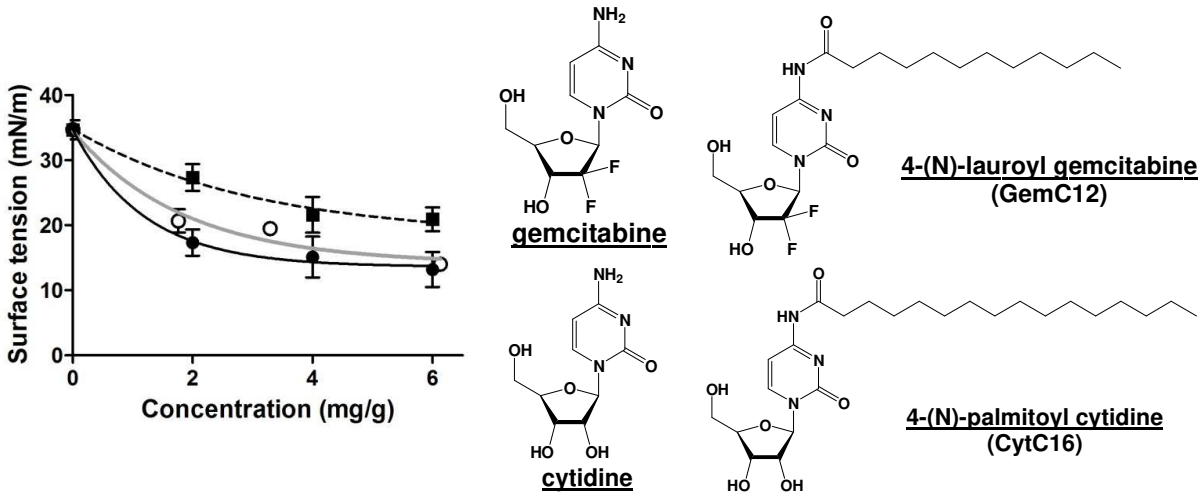

Fig. 1. Amphiphilic properties of crosslinking agents. Surface tension of the Labrafac/water interface of a 5-µL Labrafac drop in water *versus* that of GemC12 (○, grey line), CytC14 (■, dot line), and CytC16 (●, black line) at various concentrations (n = 3, mean ± SD), and chemical structures of gemcitabine, cytidine, 4-(N)-lauroyl gemcitabine (GemC12) and 4-(N)-palmitoyl cytidine (CytC16).

3.2. Design of LNC-based hydrogels using CytC16

Four protocols for LNC formulation were used, allowing to achieve various LNC size distributions: Z-ave values of 25, 50, 75, and 100 nm, with PdI values < 0.1. These protocols were defined using the mathematical modelization reported in the Supplementary discussion - Modelization of the size of LNCs. CytC16 was added at a concentration from 1 to 5% ($w/w_{Labrafac}$) during the LNC formulation process (phase inversion with temperature) and hydrogels were obtained for the targeted LNC size distributions of 50, 75, and 100-nm Z-ave after storage of the final suspensions at 4°C. Only a viscous suspension was achieved for the 25-nm LNC size. The measured size distribution of the LNCs without CytC16 confirmed the relevance of the experimental design (Table 1). Before the completion of gelation, LNCs with Cyt16 were also obtained with a size distribution and surface characteristics similar to those without CytC16 (reported for 2.5% ($w/w_{Labrafac}$) in Table 1). The addition of CytC16 did not interfere with the formulation process of the LNCs. The slight decrease in Z-ave values, greater for the largest size, can be explained by the surfactant character of CytC16 and thus an increase in the total amount of surfactant for the same amount of oil in the formulation.

Table 1. Size distributions (Z-average, Z-ave; and polydispersity index, PdI) **and surface characteristics** (Zeta potential, ZP) **for LNCs** (4 selected protocols for target sizes from 25 to 100 nm), loaded or not with 2.5% CytC16 ($w/w_{Labrafac}$), before the completion of gelation (n = 3-12, mean ± SD).

	no CytC16			**CytC16 2.5% ($w/w_{Labrafac}$)**		
Size targets	**Z-ave (nm)**	**PdI**	**ZP (mV)**	**Z-ave (nm)**	**PdI**	**ZP (mV)**
25 nm	25 ± < 1	0.08 ± 0.04	-2 ± 2	25 ± < 1	0.04 ± 0.01	-2 ± 1
50 nm	56 ± 2	0.06 ± 0.03	-4 ± 2	51 ± 3	0.06 ± 0.04	-4 ± 2
75 nm	76 ± 2	0.07 ± 0.02	-3 ± 1	71 ± 10	0.06 ± 0.01	-4 ± 2
100 nm	107 ± 4	0.09 ± 0.02	-4 ± 1	88 ± 6	0.08 ± 0.02	-3 ± 2

We measured the encapsulation rate of CytC16 after the completion of gelation for various LNC-based hydrogels (Z-ave values of 50 and 100 nm; CytC16 of 1 and 2.5% ($w/w_{Labrafac}$). The total amount of CytC16 initially added before the formulation process was retained, regardless of the LNC-based hydrogel, meaning that the phase inversion temperature protocol did not alter the CytC16 molecule (Table 2).

Table 2. Encapsulation rate of CytC16 in LNCs after the completion of gelation. CytC16 concentration measured after hydrogel dissolution and LNC solubilization by LC/MS/MS (n = 3, mean ± SD).

		CytC16 concentration (mg/mL)		
Target LNC Size	**CytC16 ($w/w_{Labrafac}$)**	**Theoretical**	**Measured**	**Encapsulation rate (%)**
50 nm	2.5%	4.78 ± 0.08	4.88 ± 0.39	102 ± 9
	1%	1.90 ± 0.01	2.03 ± 0.11	107 ± 5
100 nm	2.5%	7.68 ± 0.08	7.58 ± 0.34	99 ± 3
	1%	3.15 ± 0.04	3.03 ± 0.05	96 ± 1

We performed confocal microscopy experiments to visualize the LNC tridimensional network using DiO-loaded LNC-based hydrogels. DiO-loaded LNC suspensions (Z-ave values of 50 and 100 nm) were first analyzed (Fig. 2A and 2C). Regardless of the LNC size, no nanosystem could be detected in the confocal microscopy images due to the lack of resolution and only a diffuse

fluorescent background could be observed. However, some networks could be visualized for DiO-loaded LNC-based hydrogels, proving the interaction between the LNCs by random assembly (Fig. 2B and 2D). No conclusions could be drawn concerning the network structure or size of the LNCs in the hydrogel structure.

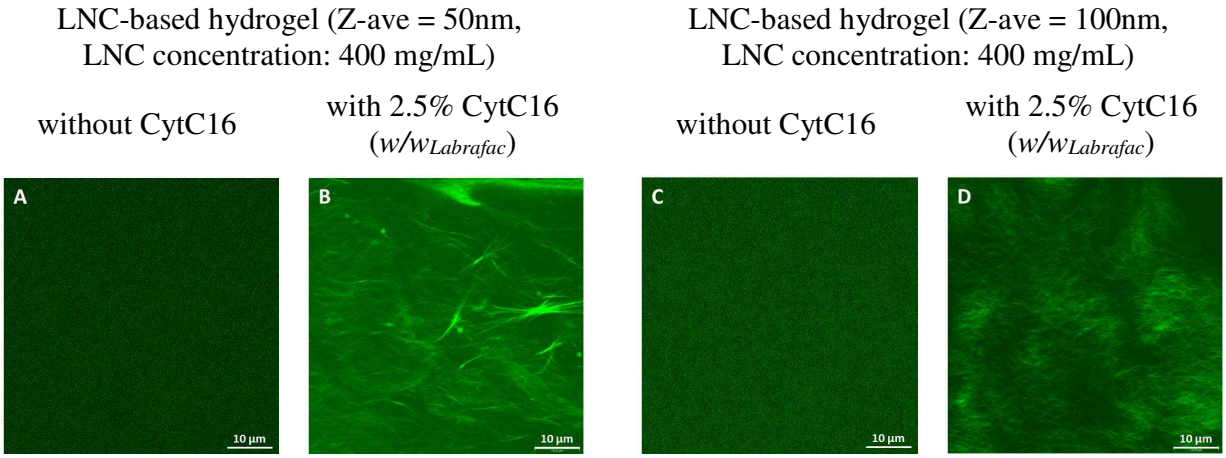

Fig. 2. Visualization of LNC-based hydrogel networks. Confocal microscopy images for (A/C) LNC suspensions and (B/D) LNC-based hydrogels (2.5% CytC16 (*w/w*$_{Labrafac}$). LNC Z-ave = 50nm (A/B) and 100 nm (B/D). LNC concentration: 400 mg/mL, 0.1% DiO (*w/w*$_{Labrafac}$).

We next measured the viscoelastic properties of the LNC-based hydrogels after the completion of gelation. First, the linear regime for the viscoelastic properties was determined, changing the oscillatory strain amplitude at a constant oscillation frequency of 1 Hz. All the hydrogels showed a linear regime, corresponding to strain-independent elastic (G') and viscous (G'') moduli up to critical oscillatory strain amplitude values of approximately 0.3%, regardless of the LNC-based hydrogel parameters. Beyond this critical value, the G' and G'' decreased. A representative profile for the determination of the linear regime is presented in Fig. S3A for a LNC-based hydrogel with 2.5% CytC16 (*w/w*$_{Labrafac}$), LNC concentration of 400 mg/mL and LNC Z-ave = 50 nm.

We, then, studied the viscoelastic properties of the gels at 25°C, within the linear regime (oscillatory strain amplitude value of 0.1%), as a function of the oscillation frequency. Constant values for G' and G'', with higher values for G' than G'', were obtained from 0.1 to 10 Hz, characteristic of a gel state. These viscoelastic properties were compared to those of LNC

suspensions, measured at the same oscillatory strain amplitude value of 0.1%, showing clear differences between the hydrogel and suspensions in terms of their mechanical properties. Representative profiles for G' and G'' *versus* the oscillation frequency are presented in Fig. S3B for LNC suspensions (no CytC16) or LNC-based hydrogels (2.5% CytC16 ($w/w_{Labrafac}$)) for LNC concentration of 400 mg/mL and LNC Z-ave = 50 nm. Then, we compared the viscoelastic properties of the LNC-based hydrogels according to the various formulation parameters at oscillatory strain amplitude of 0.1% and oscillation frequency of 1 Hz.

First, we studied the influence of the LNC concentration on the viscoelastic properties of the LNC-based hydrogels. The LNC concentrations can be adjusted by adding various volumes of cold water during the phase inversion zone of the third cooling step. Decreasing the LNC concentration in the LNC-based hydrogels (Z-ave value = 50 nm; 2.5% CytC16 ($w/w_{Labrafac}$)) led to a decrease in the G' and G'' values until a LNC concentration of approximately100 mg/mL (Fig. 3A). Lower LNC concentrations led to the loss of the hydrogel structure, with a highly viscous system that could flow. Despite the loss of hardness of the hydrogel with the decrease in LNC concentration, the high hydrogel elasticity (illustrated by the G' to G'' ratio: mean ± SD) remained constant: approximately 4 ± 1, 5 ± 1, 8 ± 1, and 12 ± 7 for LNC concentration of 400, 300, 200, and 100 mg/mL, respectively. We observed the same behavior with LNC-based hydrogels for which the LNC Z-ave were 75 and 100 nm (Fig. S4B and S4C). Gel hardness decreased with a decrease in LNC concentration in the hydrogels until a LNC concentration of approximately 100 mg/mL, from which point the hydrogels (or more precisely suspensions) began to flow. Nevertheless, the hydrogel elasticity remained constant and comparable to those for hydrogels with LNC Z-ave of 50 nm: approximately 6 ± 1, 8 ± 1 and 8 ± 2 for hydrogels with LNC Z-ave of 75 nm and approximately 6 ± < 1, 8 ± 1, and 8 ± 6 for hydrogels with LNC Z-ave of 100 nm, for LNC concentration of 300, 200, and 100 mg/mL, respectively. No gel property was obtained at LNC concentration of 300 mg/mL and lower for LNC-based hydrogels with a LNC Z-ave of 25 nm: G' and G'' values lower than 1 Pa for both (Fig. S4A) and a suspension that flowed.

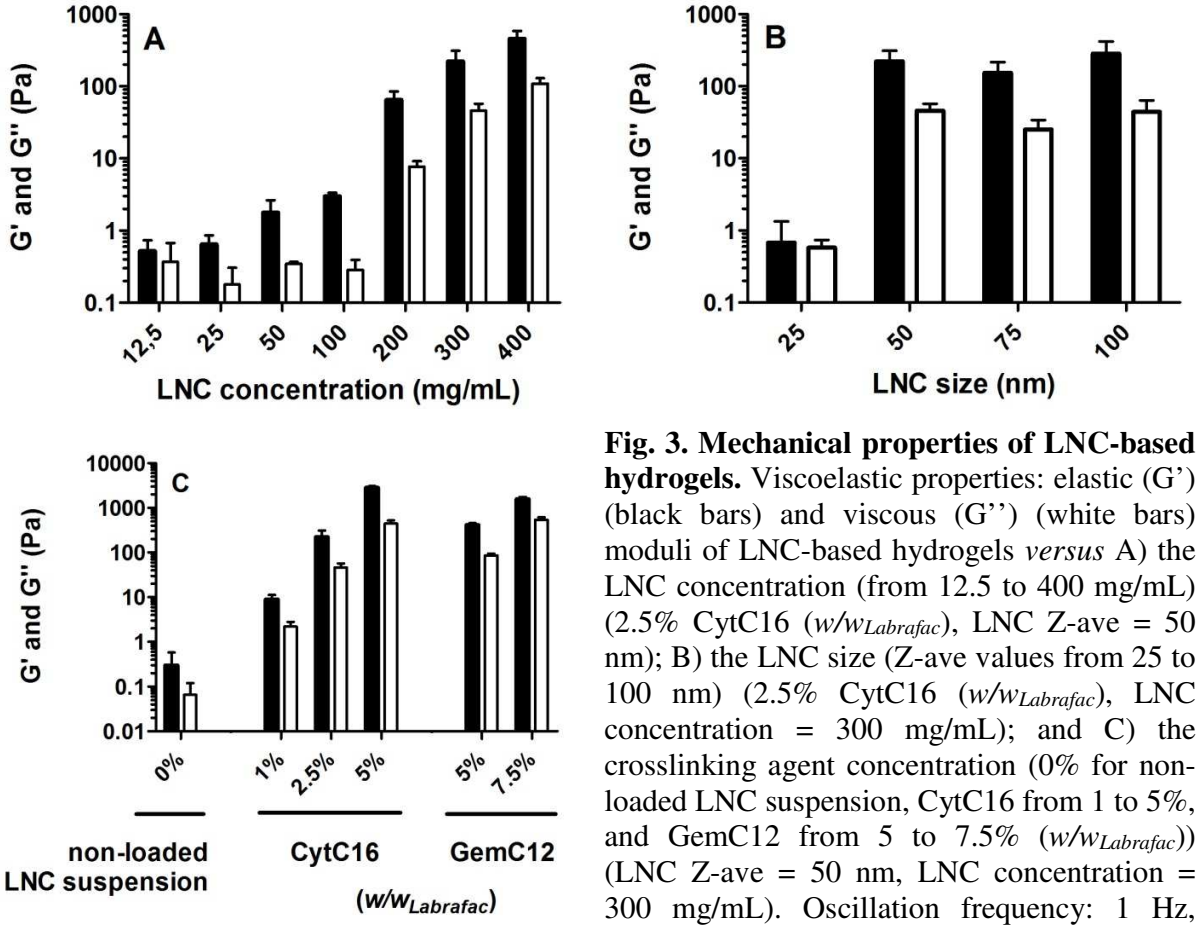

Fig. 3. Mechanical properties of LNC-based hydrogels. Viscoelastic properties: elastic (G') (black bars) and viscous (G'') (white bars) moduli of LNC-based hydrogels *versus* A) the LNC concentration (from 12.5 to 400 mg/mL) (2.5% CytC16 ($w/w_{Labrafac}$), LNC Z-ave = 50 nm); B) the LNC size (Z-ave values from 25 to 100 nm) (2.5% CytC16 ($w/w_{Labrafac}$), LNC concentration = 300 mg/mL); and C) the crosslinking agent concentration (0% for non-loaded LNC suspension, CytC16 from 1 to 5%, and GemC12 from 5 to 7.5% ($w/w_{Labrafac}$)) (LNC Z-ave = 50 nm, LNC concentration = 300 mg/mL). Oscillation frequency: 1 Hz, oscillatory strain amplitude: 0.1%, T = 25°C. (n = 3-5, mean ± SD).

Except for a LNC Z-ave of 25 nm, the LNC size did not influence the viscoelastic properties of the LNC-based hydrogels for constant LNC and CytC16 concentrations. The G' and G'' values remained constant for 2.5% CytC16 ($w/w_{Labrafac}$) and a LNC concentration of 300 mg/mL, regardless of the LNC Z-ave (50, 75 and 100 nm), with constant elasticity parameters: 5 ± 1, 6 ± 1, and 6 ± < 1, respectively (Fig. 3B). We also observed constant G' and G'' values for LNC-based hydrogels at 1% CytC16 ($w/w_{Labrafac}$) and a LNC concentration of 300 mg/mL, regardless of the LNC Z-ave (50, 75 and 100 nm), with constant elasticity parameters: 4 ± 1, 3 ± 1, and 6 ± <1, respectively (Fig. S4D).

Finally, the G' and G'' profiles were dependent on the CytC16 concentration (Fig. 3C). When the LNC concentration was 300 mg/mL and the LNC Z-ave 50 nm, the G' and G'' values increased

by more than 10 fold when CytC16 increased from 1 to 2.5% and by approximately 10 fold when it increased from 2.5% to 5% ($w/w_{Labrafac}$). The elasticity parameter remained constant: 4 ± 1, 5 ± 1, and 6 ± 1 for 1%, 2.5% and 5% CytC16 ($w/w_{Labrafac}$), respectively. Comparison with GemC12-loaded LNC-based hydrogels showed similar viscoelastic properties with higher GemC12 concentrations. Indeed, LNC-based hydrogels with 2.5% CytC16 and 5% GemC12 ($w/w_{Labrafac}$) have the same mechanical properties, as do those with 5% CytC16 and 7.5% GemC12 ($w/w_{Labrafac}$) (Fig. 3C).

3.3. Properties of LNC-based hydrogels using CytC16: release profiles, stability, and injectability.

We performed *in vitro* LNC-based hydrogel dissolution studies to follow the release of LNCs and/or model drugs from the LNC-based hydrogel into an artificial extracellular matrix at 37°C under static conditions (without stirring). Rapid dissolution occurred when the LNC-based hydrogels with 2.5% CytC16 ($w/w_{Labrafac}$) were in contact with the artificial extracellular matrix. Measurement of the fluorescence of NR-loaded LNCs showed up to 100% to be in suspension after three days (Fig. 4A). Slower dissolution was observed for the LNC-based hydrogels with 5% CytC16 ($w/w_{Labrafac}$), with approximately 50% of LNCs in suspension after three days. Dissolution was inhibited by the static condition between three days and one week. Subsequent stirring led to dissolution of the LNC-based hydrogel (data not shown). Interestingly, the same release profiles were observed for LNC-based hydrogels with 5% and 7.5% GemC12 ($w/w_{Labrafac}$), respectively (Fig. 4A).

While NR was used to mimic a lipophilic drug (in the LNC core) and to follow the LNCs as a tag, fluorescein was used to mimic a hydrophilic drug, solubilized in the aqueous environment of the LNC-based hydrogel. The total release of fluorescein was very rapid and occurred without total dissolution of the hydrogel. The whole fluorescein was released within a few hours when the LNC-based hydrogels were placed in contact with the artificial extracellular matrix, regardless of the CytC16 concentration in the LNC-based hydrogels: from 1 to 5% ($w/w_{Labrafac}$) (Fig. 4B).

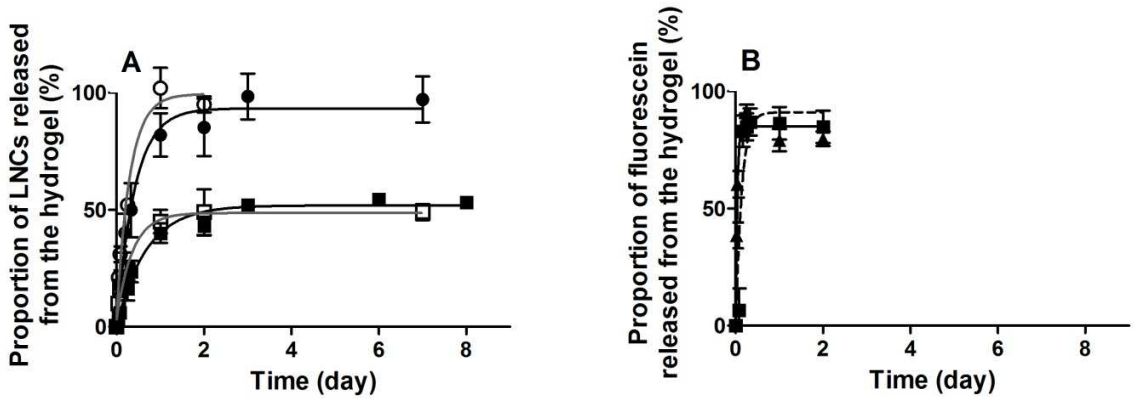

Fig. 4. Progressive dissolution of LNC-based hydrogels. Release of A) NR-loaded LNCs and B) fluorescein from LNC-based hydrogels (LNC concentration = 300 mg/mL, LNC Z-ave = 50 nm, 0.1% NR ($w/w_{Labrafac}$), 0.1 mg/mL fluorescein in LNC-based hydrogels) into an artificial extracellular matrix at 37°C, without stirring. CytC16 concentrations of 1% (▲), 2.5% (●), and 5% ($w/w_{Labrafac}$) (■) or GemC12 concentrations of 5% (○) and 7.5% ($w/w_{Labrafac}$) (□). LNC-based hydrogel volume of 300 µL in an artificial extracellular matrix of 5.7 mL (n = 3, mean ± SD).

This innovative gel form could be directly stored in syringes as part of its pharmaceutical development before subcutaneous or local injection of patients. The LNC-based hydrogels appeared to be relatively stable as no change in its viscoelastic properties were observed over six months (Fig. 5A). Nevertheless, the initial LNC size distributions were modified after total dissolution of the LNC-based hydrogels, with an increase in the Z-ave and PdI values. The maximal Z-ave values were approximately 150 nm, with PdI values close to 0.2 (Fig. 5B) several months after storage at 4°C, indicating i) destabilization of the LNCs in the LNC hydrogel forms or ii) partial dissolution of the LNC-based hydrogels, with a number of LNC clusters. The second assumption is relevant because the size distributions of LNCs were measured during the release studies (fresh LNC-based hydrogels used for this purpose) and deviations from the size distribution were also observed. The total dissolution of LNC-based hydrogels (LNC concentration = 300 nm; Z-ave = 50nm) with CytC16 concentrations of 1, 2.5, and 5% ($w/w_{Labrafac}$) led to size distribution values for Z-ave (mean ± SD) and PdI (mean ± SD) of 80 ± 4 nm and 0.30 ± 0.03, 120 ± 40 nm and 0.38 ± 0.04, and 90 ± 19 nm and 0.39 ± 0.05, respectively. In addition, the total dissolution of LNC-based hydrogels (LNC concentration = 300 nm; Z-ave = 100 nm) with CytC16 concentrations of 1, 2.5 and 5% ($w/w_{Labrafac}$) led to size distribution values

for Z-ave and PdI of 167 ± 26 nm and 0.38 ± 0.06, 145 ± 20 nm and 0.42 ± 0.06, and 183 ± 77 nm and 0.61 ± 0.16, respectively.

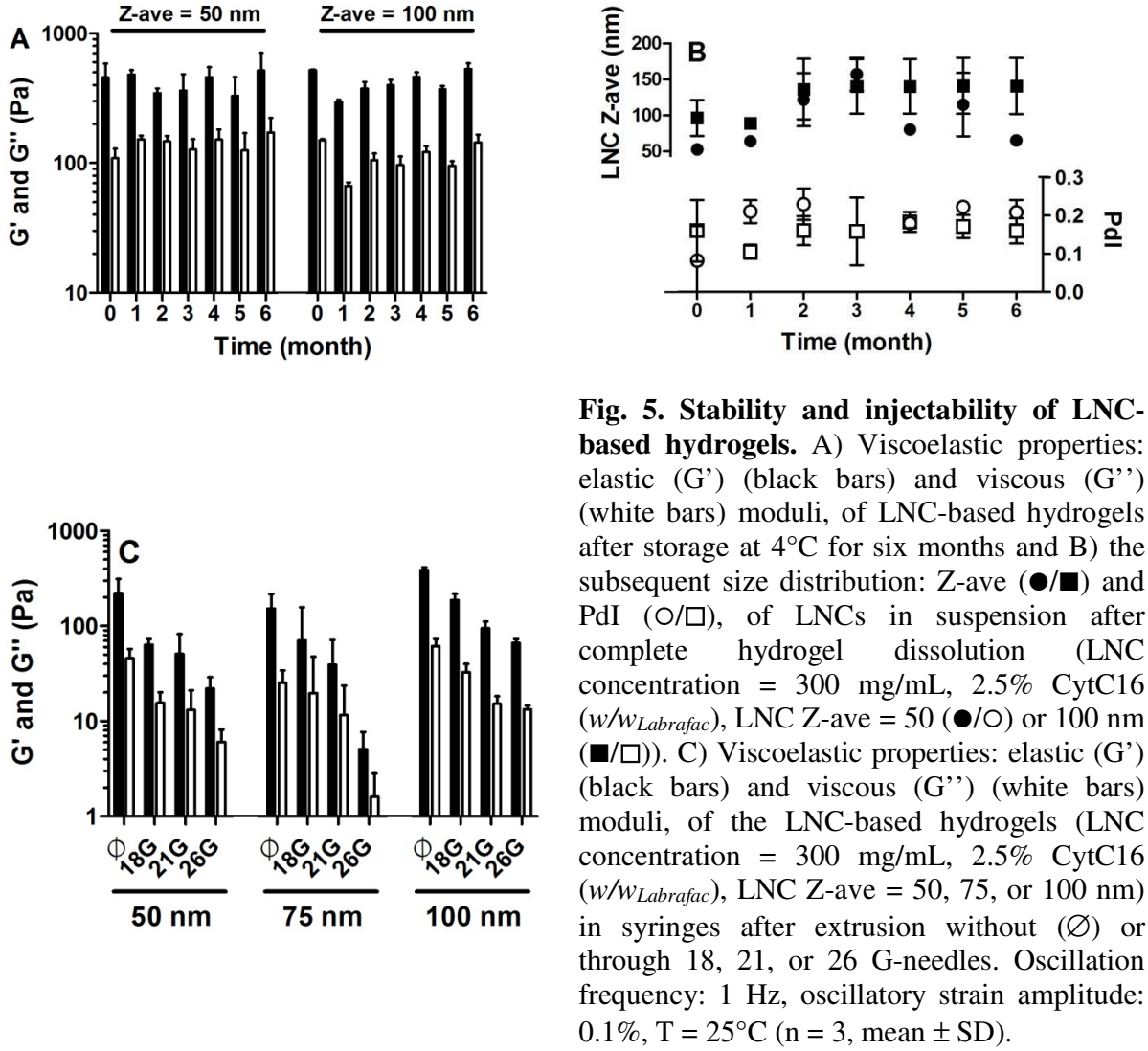

Fig. 5. Stability and injectability of LNC-based hydrogels. A) Viscoelastic properties: elastic (G') (black bars) and viscous (G'') (white bars) moduli, of LNC-based hydrogels after storage at 4°C for six months and B) the subsequent size distribution: Z-ave (●/■) and PdI (○/□), of LNCs in suspension after complete hydrogel dissolution (LNC concentration = 300 mg/mL, 2.5% CytC16 ($w/w_{Labrafac}$), LNC Z-ave = 50 (●/○) or 100 nm (■/□)). C) Viscoelastic properties: elastic (G') (black bars) and viscous (G'') (white bars) moduli, of the LNC-based hydrogels (LNC concentration = 300 mg/mL, 2.5% CytC16 ($w/w_{Labrafac}$), LNC Z-ave = 50, 75, or 100 nm) in syringes after extrusion without (∅) or through 18, 21, or 26 G-needles. Oscillation frequency: 1 Hz, oscillatory strain amplitude: 0.1%, T = 25°C (n = 3, mean ± SD).

The filling of syringes before the completion of gelation was performed. Once gelation was achieved inside the syringe (storage at 4°C overnight), the LNC-based hydrogels were then directly extruded without or through 18 to 26 G-needles. The viscoelastic properties decreased progressively as the needles became thinner, regardless of the LNC size of the LNC-based hydrogels (Fig. 5C). Interestingly, the LNC-based hydrogels could be extruded through needles

down to 26 G and although the gel hardness decreased, the elasticity was retained: 4 ± < 1, 4 ± 1, and 5 ± < 1 for the LNC-based hydrogels (LNC concentration = 300 mg/mL, 2.5% CytC16 ($w/w_{Labrafac}$)) with an LNC Z-ave of 50, 75, and 100 nm, respectively.

3.4. CytC16 cytotoxicity and *in vivo* behavior of LNC-based hydrogels after subcutaneous administration.

The safety of CytC16 was determined by measuring its cytotoxic effect. Due to its solubility profile, CytC16 was solubilized in DMSO prior to incubation with macrophages (THP1 cell line) at various concentrations in culture medium. The CytC16 concentrations tested were limited by its solubility in DMSO and cell culture medium mixture. We observed 100 % cell viability for CytC16 concentration from approximately 1 to 10 µg/mL (Fig. S5).

We, then, compared incubation of macrophages with CytC16-loaded LNCs (after LNC-based hydrogel dissolution) to incubation with LNC suspensions without CytC16 at the same concentration to be sure that any cytotoxicity of CytC16 associated with the LNCs was not additional. The half-maximal inhibitory concentration (IC50) values (mean ± SD) were 1.62 ± 0.12 and 2.17 ± 0.09 mg/mL when macrophages (THP1 cell line) were incubated with CytC16-loaded (2.5% CytC16 ($w/w_{Labrafac}$)) and non-loaded LNC suspensions (Z-ave = 50 nm), respectively. The slightly but significantly ($p < 0.05$) lower IC50 value for CytC16-loaded LNCs *versus* non-loaded LNCs was not observed with a Z-ave = 100 nm. The IC50 values were 2.08 ± 0.15 and 2.36 ± 0.16 mg/mL when the cells were incubated with CytC16-loaded (2.5% CytC16 ($w/w_{Labrafac}$)) and non-loaded LNC suspensions, respectively (Fig. 6A).

We incubated LNC suspensions with another cell type (pancreatic cells: B6-KPC3 cell line) to verify that the addition of Cyt-C16 to LNCs did not modify the IC50 values, regardless of the LNC size. The IC50 values were 1.16 ± 0.14 and 1.35 ± 0.21 mg/mL when the cells were incubated with CytC16-loaded (2.5% CytC16 ($w/w_{Labrafac}$)) and non-loaded LNC suspensions (Z-ave = 50 nm), respectively, and 1.51 ± 0.24 and 1.69 ± 0.20 mg/mL when they were incubated with CytC16-loaded (2.5% CytC16 ($w/w_{Labrafac}$)) and non-loaded LNC suspensions (Z-ave = 100 nm), respectively (Fig. 6B).

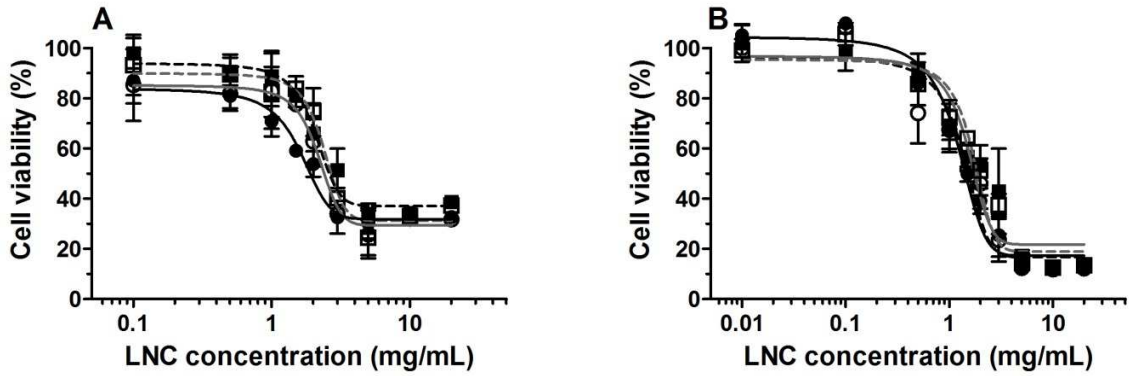

Fig. 6. Safety of CytC16-loaded LNCs. Cell viability of (A) THP1 and (B) B6-KPC3 cell lines *versus* the LNC concentration: LNC Z-ave = 50 nm, non-loaded (○, grey line) or loaded with 2.5% CytC16 ($w/w_{Labrafac}$) (●, black line) and LNC Z-ave = 100 nm, non-loaded (□, grey dot line) or loaded with 2.5% CytC16 ($w/w_{Labrafac}$) (■, black dot line), after a 48-h incubation at 37°C (n = 3, mean ± SD).

We assessed a preliminary biocompatibility profile by performing subcutaneous administration of LNC-based hydrogels (LNC concentration = 400 mg/mL, 2.5% CytC16 ($w/w_{Labrafac}$), LNC Z-ave = 50 nm) with syringes (500 µL, 18-G needle) to eight-week female rats, and compared it to the subcutaneous administration of sesame oil under the same conditions. Sesame oil is an approved excipient for drug formulation for the subcutaneous and/or intramuscular routes (Haldol Decanoas® 50 mg/mL, Janssen-Cilag; Modecate® 125 mg/mL, Sanofi-Aventis). Thus, the tissues and overall reactions caused by the LNC-based hydrogels were compared to those caused by an excipient currently accepted by the European Pharmacopoeia.

Because of its fluidity, sesame oil is less well retained and tends to leak out through the injection site, what was not observed for the LNC-based hydrogel. We observed scratching and grooming behavior at the injection site of the animals during the first 24 h after administration of the two formulas, but not beyond this period. No animal showed any change in behavior or signs of suffering and the weight profiles of the animals, considered to be the best marker of suffering, did not show any significant variation relative to that of non-treated rats (Fig. S6). The two formulations did not appear to affect the general health of the animals. Moreover, the injected forms remained visible throughout the study as a lump under the skin. The area around the injection site did not appear to be infected, erythematous, or painful. Blood samples were taken from each animal at the various times of euthanasia to determine the complete hematological

profile in fresh blood (Tables S4 and S5) and biochemical analysis of plasma (Table S6). The hematological profile was not significantly altered, regardless of the injected form or time after injection. The overall leukocyte counts appeared to slightly increase between the second and fourteenth day. However, they remained close to the normal values reported in the literature (3 x 10^9 to 15 x 10^9 /L) [28]. In addition, the distribution of the leukocyte cell types remained unchanged during the study. Finally, the values from biochemical analysis of the animals remained unchanged and were comparable to those of non-treated animals.

The tissues surrounding the implants were excised following euthanasia of each animal and thin sections stained using a hematoxylin-eosin standard protocol. The slides (Fig. 7) were compared to those made using tissues from a healthy control and a score was given for each condition (Table 3).

Table 3. Evaluation of hypoderm lesions relative to normal tissue: leucocyte infiltration, fibroblasts and collagen deposition, and neo-angiogenesis, graded from normal to high, after subcutaneous injections (500 µL) of LNC-based hydrogels (LNC concentration = 400 mg/mL, 2.5% CytC16 ($w/w_{Labrafac}$), LNC Z-ave = 50 nm) or sesame oil to Sprague-Dawley female rats after 1 to 28 days (n = 3).

Time	Implant	Leucocyte infiltration	Fibroblasts and collagen deposition	Neo angiogenesis
1 day	Sesame oil	+++	∅	∅
	LNC-based hydrogel	+++	∅	∅
2 days	Sesame oil	+++	∅	∅
	LNC-based hydrogel	+++	∅	∅
4 days	Sesame oil	+++	+/-	+/-
	LNC-based hydrogel	+++	+/-	∅
7 days	Sesame oil	++	++	+
	LNC-based hydrogel	++	++	+
14 days	Sesame oil	+	+++	++
	LNC-based hydrogel	+	+++	+++
28 days	Sesame oil	+/-	+++	++
	LNC-based hydrogel	+/-	+++	+++

∅: normal, +/-: minimum, +: medium, ++: moderate, +++: high

We observed an acute inflammatory reaction for all the implants from the first 24 h. The area that contained the injected form was clearly visible. This ovoid cavity was empty of any structure. Indeed, the tissue preparation steps led to elimination of the formula and no living tissue had infiltrated into the space. The inflammatory reaction resulted in the recruitment of numerous leukocytes around the injection site. These cells mainly consisted of neutrophilic granulocytes and a few eosinophilic granulocytes. The closer the cells were to the margins of the cavity, the more concentrated they were. Surrounding tissues also showed interstitial edema, which appeared to be slightly more prominent for the LNC-based hydrogel. After 48 h, the cavities containing the formulations were still well delineated and granulocyte recruitment continued (Fig. 7, day 2).

From the fourth day of observation, the number of leukocytes in the tissues stabilized and fibroblasts started to appear. After one week, the granulocytes began to decrease and gave way to macrophages and fibroblasts multiplied around the space of implant. The injection area of the sesame oil maintained the same aspect of an empty and well delimited cavity, but the aspect of the space containing the LNC-based hydrogel changed. Indeed, the cavity fragmented into several large vacuoles between which living tissue infiltrated (Fig. 7, day 7).

On the fourteenth day, the cavity that contained the sesame oil was still visible and empty. The cavity created by the LNC-based hydrogel showed increasing infiltration by the extracellular matrix and a small number of cells. The cavities, empty or not, were surrounded by a fibrous capsule composed of fibroblasts and collagen deposits. A few leukocytes, mainly mononuclear cells (macrophages and lymphocytes), were still found in and around the capsule but their number remained moderate. In addition, newly formed blood capillaries were observed around the implant (Fig. 7, day 14).

At the end of the study, four weeks after the subcutaneous administration, the cavity containing the sesame oil was still well defined, acellular, and surrounded by a fibrous capsule. The cavity created by the LNC-based hydrogel, on the other hand, showed increasing fragmentation and cell infiltration, but the injection area was also surrounded by a fibroblast capsule (Fig. 7, day 28).

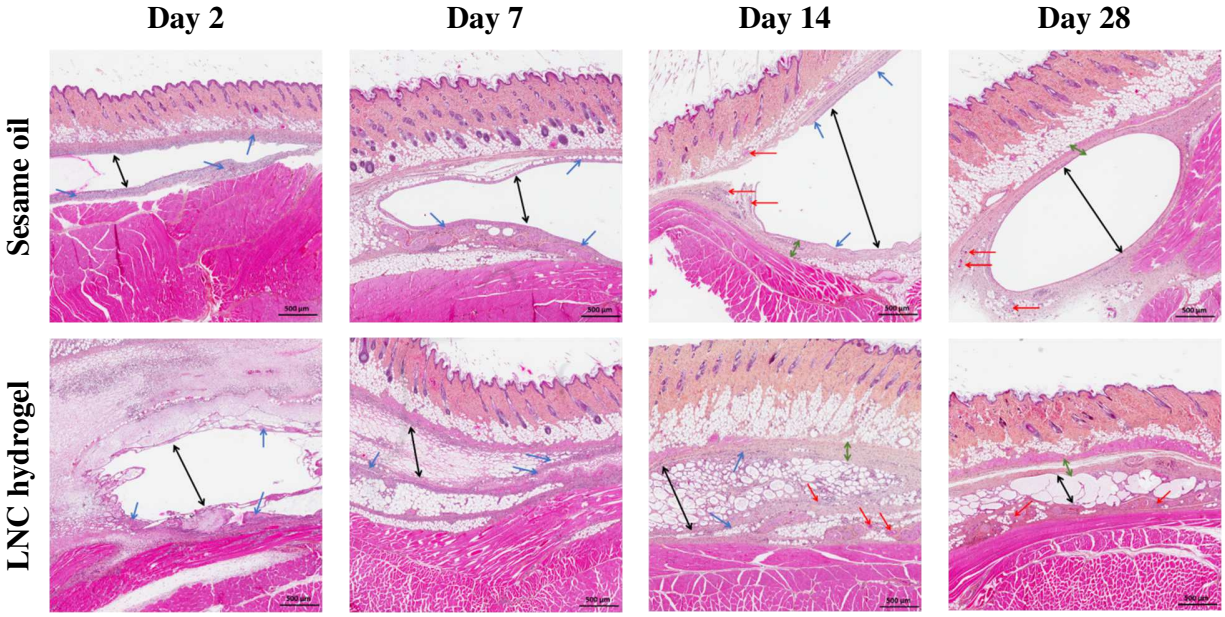

Fig. 7. Histological images of the implant surrounding tissues. Microscopic sections of Sprague-Dawley female rat subcutaneous tissues 2, 7, 14, and 28 days after subcutaneous injections (500 µL) of LNC-based hydrogels (LNC concentration = 400 mg/mL, 2.5% CytC16 ($w/w_{Labrafac}$), LNC Z-ave = 50 nm) or sesame oil. The implant area (black arrow), leucocytes (blue arrow), blood vessels (red arrow), and fibrosis (green arrow) are indicated.

4. DISCUSSION

Although not new, hydrogels are a pharmaceutical dosage form that still has its place in the therapeutic arsenal. Numerous studies have reported the therapeutic efficacy of these drug delivery systems when loaded with nanoparticles after local administration [21]. This pharmaceutical platform combines the advantages of the two technologies: i) the pharmacological properties of the API dictated by the fate of the nanoparticles, passive or active targeting, and the opportunity to combine APIs; and ii) local administration and sustained release provided by the hydrogels.

In the recent literature, the design of nanoparticle-loaded hydrogels has remained the same, with the dispersion of the nanoparticles in a natural or synthetic matrix that forms the hydrogel [21]. New designs could be considered to improve this drug delivery system, as we report in this study: a hydrogel of nanoparticles without the use of a polymer. Several recent studies have already explored this new concept and interesting applications were proposed. Wang, *et al*, developed

poly (lactide-co-glycolide) (PLGA) nanoparticles and modified their surface with a coating of poly (ethylene-co-maleic acid) (PEMA) or polyvinyl amine (PVAm). Thus, PLGA nanoparticles were obtained with opposite surface charges: zeta potential values of -20 ± 1 and +30 ± 1 mV for PLGA-PEMA and PLGA-PVAm nanoparticles, respectively, with similar sizes (diameters of 180 ± 15 and 145 ± 10 nm, respectively). When the polymeric nanoparticles were mixed, a gel was obtained by electrostatic interactions between the nanoparticles of opposite charges. This drug delivery system was used in bone repair, with the encapsulation of dexamethasone in the nanoparticles. This API promotes osteogenesis and bone formation was stimulated by the release of dexamethasone after application of the PLGA nanoparticle-based gel in a mouse model of bone defect [29]. Gu, *et al*, proposed the use of dextran nanoparticles with different coatings: chitosan to have positively charged nanoparticles or alginate to have negatively charged ones (zeta potential values of +11 ± 2 and -12 ± 2 mV, respectively, with similar sizes: 340 and 290 nm, respectively). As in the previous study, a gel was formed after mixing the two nanoparticle suspensions, still without the presence of a polymer to form a three-dimensional network, but only by self-association of the nanoparticles through electrostatic interactions [30]. This drug delivery system was used as an intelligent insulin-releasing implant, stimulated by the hyperglycemic context, for the treatment of type 1 diabetes. Subcutaneous administration of the nanoparticle-based hydrogel loaded with insulin and glucose-specific enzymes maintained a normal blood glucose concentration (< 2 g/L) for up to 10 days in an induced diabetes mouse model, demonstrating that the release of insulin was triggered by hyperglycemia. On the contrary, blood glucose levels remained abnormally high after subcutaneous administration of insulin solution or nanoparticle-based hydrogel loaded with only insulin or only glucose-specific enzymes (at equivalent doses).

In addition to the highly relevant applications for these drug delivery systems, these two studies present a new design for nanoparticle-based hydrogel systems without a polymer network. Similarly, we focused on the development of a new design for LNC-based hydrogels using GemC12 as a crosslinking agent. The LNCs auto-associated to form a three-dimensional network, without using a polymer, through H-bonds due to the gemcitabine moieties of GemC12 at their surface [23]. The antimetabolite property of the GemC12 molecule allowed the use of the LNC-based hydrogels for anticancer applications i) after subcutaneous administration to treat the mediastinal metastases of lung primary tumors [24], or ii) by filling the resection cavity after

glioblastoma surgery (clinical protocol when surgery is possible) to treat tumor recurrences [25-27]. Gemcitabine was replaced by the endogenous nucleoside analog cytidine for the development of this drug delivery system as a general platform.

The modification of cytidine was a milestone. Indeed, the lauroyl-modification of cytidine (CytC12) did not lead to amphiphilic properties similar to those of GemC12. Modification with a longer aliphatic chain was thus performed to obtain the hydrophilic-lipophilic balance of GemC12. Indeed, the hydrophilic character of cytidine should be higher than that of gemcitabine due to an additional hydroxyl function on the cytidine cycle, and CytC16 and GemC12 showed similar amphiphilic properties at the oil/water interface (Fig. 1).

CytC16-loaded LNC-based hydrogels have properties comparable to those loaded with GemC12 [23]. The viscoelastic properties of the LNC-based hydrogels increased with increasing LNC and/or crosslinking agent concentrations (GemC12 or CytC16) (Fig. 3A and C, respectively). With an unchanging LNC volume fraction, the size of the LNCs did not modify the viscoelastic properties (Fig. 3B). The LNC-based hydrogels could be injected using syringes and needles with only a slight loss of the viscoelastic properties after extrusion (Fig. 5C). In addition, hydrogel dissolution led to the sustained release of LNCs (Fig. 4A). There were several differences in terms of the values of the viscoelastic moduli. The concentrations of CytC16 must be lower than those of GemC12 to reach viscoelastic properties similar to those of GemC12-loaded LNC-based hydrogels. Similar G' and G'' values for LNC-based hydrogels were observed with 2.5% CytC16 and 5% GemC12 (w/w_{Lab}) or 5% CytC16 and 7.5% GemC12 (w/w_{Lab}) (Fig. 3C). The auto-association between LNCs occurred through H-bonds. The enhanced viscoelastic properties of the CytC16-loaded LNC-based hydrogels might be due to the additional hydroxyl function of the cytidine moieties at the surface of the LNCs. In addition, we showed that the LNC release profiles are mediated by the viscoelastic properties of the LNC-based hydrogels. Similar LNC release profiles were observed with 2.5% CytC16 and 5% GemC12 (w/w_{Lab}) and 5% CytC16 and 7.5% GemC12 (w/w_{Lab})-loaded LNC-based hydrogels (Fig. 4A).

CytC16 appears to be a good candidate for the development of the LNC-based hydrogel as a platform for drug delivery in terms of its interactions with biological media (*in vitro* and *in vivo*). The CytC16 crosslinking agent, composed of an endogenous molecule, did not lead to additional toxicity over that of blank LNCs (Fig. 6). In previous studies, the same assays were carried out

with GemC12-loaded LNCs for various other cell lines (Mia PaCa-2 and BxPc-3, pancreatic tumors; H460 and Ma44-3, lung tumor; U-87MG, U251, T98G, GL261, C6, 9L and 9L-lacZ: glioblastoma) [23-27,31]. The IC50 values obtained for LNCs with GemC12 were reduced by at least 50-fold relative to LNCs without GemC12. During the week following the subcutaneous administration of CytC16-loaded LNC-based hydrogels, a first phase of acute inflammation was induced, followed by a sub-chronic/chronic phase. This inflammatory reaction was local and showed no sign of associated severity. The trauma induced by the passage of the needle during the injection also participated in triggering the acute inflammation. In addition, the forms used were made under clean but not perfectly aseptic conditions, which may also have increased the inflammatory reaction. The reactions caused by the LNC-based hydrogels appeared to be acceptable: the development of fibrosis around the implants was common and could be attributed to inflammatory reactions to foreign body, and the control composed of sesame oil, an excipient approved for parenteral injection, provoked the same reactions (Table 3 and Fig. 7). In the literature, other implants, such as organogels based on safflower oil, produced and administered under aseptic conditions showed a foreign-body inflammatory response after subcutaneous administration, comparable in intensity to that observed for the LNC-based hydrogel [32].

This study was conducted over a period of one month, which was not sufficient to observe the complete degradation of the injected CytC16-loaded LNC-based hydrogels. A longer-term study to assess the fate of the LNC hydrogels, as well as healing of the surrounding tissues, would be informative. In addition, various additional *in vitro* and *in vivo* studies will be necessary to determine the true safety of such LNC-based hydrogels: genotoxicity tests, oxidative stress assays, bio-persistence, carcinogenicity, and pharmacokinetic studies (distribution, metabolism, and excretion) (AFFSAPS recommendation: 2nd edition, https://ansm.sante.fr/var/ansm_site/storage/original/application/7042aee471537987a082180039a5bded.pdf , accessed January 4, 2021). Finally, the infiltration of the extracellular matrix (Fig. 7) into the LNC hydrogel implant can be explained by its dissolution and thus the release of LNCs observed with the *in vitro* assays (Fig. 4A). It is important to note that only the viscoelastic properties (based on both the crosslinking agent and LNC concentrations) mediate the release profiles of the LNC. Nevertheless, the release profile of hydrophilic molecules was not affected by the viscoelastic properties of the LNC-based hydrogels (Fig. 4B). This interesting aspect would be useful in promoting sequential release of different types of APIs: hydrophilic in the

matrix and lipophilic in the LNC core. One limitation of this LNC-based hydrogel design is the loss of stability during storage in terms of LNC size (Fig. 5B), despite the stable viscoelastic properties (Fig. 5A). This result also confirms that LNC size has no effect on the viscoelastic properties (Fig. 3B). The observed changes in size would affect the distribution of the LNCs after dissolution of the LNC-based hydrogel. This aspect requires further exploration.

In summary, the LNC-based hydrogels have all the characteristics and properties of conventional nanoparticle hydrogels, except the absence of a polymer network. These new platform for drug delivery could be useful for the development of new therapeutic practices, in particular for local or subcutaneous administration. For example, numerous studies have reported the use of nanoparticles in immunology after subcutaneous administration [33-36]. Pitorre, *et al*, already showed the relevance of the subcutaneous administration of LNCs to target specific lymph nodes, depending on the injection sites [37], and the use of LNC-based hydrogels to prolong lymph-node accumulation could open up new research opportunities. Another example could be the implementation of this drug delivery platform for ocular administration. Nanoparticles have already been tested against glaucoma and retinoblastoma [38,39]. However, a limitation for the translation of this approach is the limited local resident time for the APIs, necessitating repeated administration of the therapy. An important perspective for therapy development is improvement of the local resident time after administration [40,41]. Certain devices have already been developed, such as Retisert® (Bausch & Lomb, United States), an intravitreal implant indicated for the treatment of chronic non infectious uveitis affecting the posterior segment of the eye. Nevertheless, an invasive implantation procedure is required. Other implanted devices are under study, such as microneedle delivery [42] or polymer matrix implants [43]. The use of nanoparticle-based hydrogels without using a polymer could be promising to limit additional toxicity inherent to the polymer used for these matrices, even using biocompatible and biodegradable macromolecules.

5. Conclusion

We developed a new crosslinking agent, CytC16, which allowed the formation of a LNC-based hydrogel without the use of a polymer. This molecule is composed of a palmitic chain covalently bound via an amide function to cytidine. The hydrogel was obtained by the creation of a network of auto-associated LNCs, like a three-dimensional pearl necklace. The higher the CytC16 concentration in the hydrogel was, the more rigid was the resulting network. Furthermore, the LNC Z-ave must be above 50 nm and increasing the LNC concentration led to increasingly rigid hydrogels. The LNC-based hydrogels were injectable and the release profiles of LNCs from the hydrogels correlated with their viscoelastic properties. Finally, the LNC-based hydrogels showed good biocompatibility based on preliminary assays after *in vivo* subcutaneous administration, with a local inflammatory response similar to those induced by an approved excipient. Due to its endogenous character, CytC16 is a highly promising crosslinking agent to obtain a LNC-based hydrogel platform for the design of drug delivery systems for multiple pharmaceutical applications.

Author contribution

Conceptualization: G.B.; Methodology: M.P., J.P.B. and G.B.; Software: J.R.; Investigation: M.P., C.G., L.T.T.P., K.F., J.B., N.L., R.P., F.G., V.M. and G.B.; Writing - Original Draft: M.P. ang G.B.; Writing - Review & Editing: J.R., R.P., F.G., V.M., J.P.B. and G.B.; Visualization: M.P., C.G., G.B.; Supervision: J.P.B. and G.B.; Project administration: G.B.; Funding acquisition: J.P.B. and G.B.

Conflict of interest

The authors declare no conflict of interest.

Acknoledgements

This work was carried out within the research program of NICHE (EuroNanoMed2 - 4th call) and GLIOGEL (EuroNanoMed3 - 7th call). The authors also thank the « Fondation ARC pour le Recherche sur le Cancer » and the « Ligue Contre le Cancer (Comité du Maine-et-Loire) » for their financial support. We thank the Pathology Department of the University Hospital of Angers for technical assistance in the hematoxylin-phloxin-saffron staining of the tissue sections.

References

[1] J. Shi, P.W. Kantoff, R. Wooster, O.C. Farokhzad, Cancer nanomedicine: progress, challenges and opportunities, Nature Reviews Cancer 17(1) (2017) 20-37.

[2] R.A. Petros, J.M. DeSimone, Strategies in the design of nanoparticles for therapeutic applications, Nature Reviews Drug Discovery 9 (2010) 615-627.

[3] E. Blanco, H. Shen, M. Ferrari, Principles of nanoparticle design for overcoming biological barriers to drug delivery, Nature Biotechnology 33 (2015) 941-951.

[4] J. Shi, Z. Xiao, N. Kamaly, O.C. Farokhzad, Self-assembled targeted nanoparticles: evolution of technologies and bench to bedside translation, Accounts of Chemical Research 44 (2011) 1123-1134.

[5] P.P. Adiseshaiah, R.M. Crist, S.S. Hook, S.E. McNeil, Nanomedicine strategies to overcome the pathophysiological barriers of pancreatic cancer, Nature Reviews Clinical Oncology 13(12) (2016) 750-765.

[6] M.E. Lobatto, V. Fuster, Z.A. Fayad, W.J.M. Mulder, Perspectives and opportunities for nanomedicine in the management of atherosclerosis, Nature Reviews Drug Discovery 10(11) (2011) 835-852.

[7] O. Veiseh, B.C. Tang, K.A. Whitehead, D.G. Anderson, R. Langer, Managing diabetes with nanomedicine: challenges and opportunities, Nature Reviews Drug Discovery 14(1) (2015) 45-57.

[8] J. Shi, A.R. Votruba, O.C. Farokhzad, R. Langer, Nanotechnology in drug delivery and tissue engineering: from discovery to applications, Nano Letters 10 (2010) 3223-3230.

[9] J.J. Kang-Mieler, W.F. Mieler, Thermo-Responsive Hydrogels for Ocular Drug Delivery, Developments in Ophthalmology 55 (2016) 104-111.
[10] R. Sheshala, Y.Y. Kok, J.M. Ng, R.R.S. Thakur, K. Dua, In Situ Gelling Ophthalmic Drug Delivery System: An Overview and Its Applications, Recent Patents on Drug Delivery & Formulation 9(3) (2015) 237-248.
[11] C. Karavasili, D.G. Fatouros, Smart materials: in situ gel-forming systems for nasal delivery, Drug Discovery Today 21(1) (2016) 157-166.
[12] C.M. Caramella, S. Rossi, F. Ferrari, M.C. Bonferoni, G. Sandri, Mucoadhesive and thermogelling systems for vaginal drug delivery, Advanced Drug Delivery Reviews 92 (2015) 39-52.
[13] M. Cully, Inflammatory diseases: Hydrogel drug delivery for inflammatory bowel disease, Nature Reviews Drug Discovery 14(10) (2015) 678-679.
[14] R.H. Koh, Y. Jin, J. Kim, N.S. Hwang, Inflammation-Modulating Hydrogels for Osteoarthritis Cartilage Tissue Engineering, Cells 9(2) (2020) 419.
[15] Y. Liu, Y.H. Hsu, A.P. Huang, S.H. Hsu, Semi-Interpenetrating Polymer Network of Hyaluronan and Chitosan Self-Healing Hydrogels for Central Nervous System Repair, ACS Applied Materials & Interfaces 12(36) (2020) 40108-40120.
[16] S.R. Feldman S. R., Principles of topical treatment: advancement in gel vehicle technology, Journal of Drugs in Dermatology 13(4) (2014) 423-427.
[17] R. Vaishya, V. Khurana, S. Patel, A.K. Mitra, Long-term delivery of protein therapeutics, Expert Opinion on Drug Delivery 12(3) (2015) 415-440.
[18] N.K. Singh, D.S. Lee, In situ gelling pH- and temperature-sensitive biodegradable block copolymer hydrogels for drug delivery, Journal of Controlled Release 193 (2014) 214-227.
[19] F.M. Chen, X. Liu, Advancing biomaterials of human origin for tissue engineering, Progress in Polymer Science 53 (2016) 86-168.
[20] L. Gu, D.J. Mooney, Biomaterials and emerging anticancer therapeutics: engineering the microenvironment, Nature Reviews Cancer 16(1) (2016) 56-66.
[21] M. Pitorre, H. Gondé, C. Haury, M. Messous, J. Poilane, D. Boudaud, E. Kanber, G. Alexis, R. Ndombina, J.P. Benoit, G. Bastiat, Recent advances in nanocarrier-loaded gels: Which drug delivery technologies against which diseases?, Journal of Controlled Release 266 (2017) 140-155.

[22] B. Heurtault, P. Saulnier, B. Pech, J.E. Proust, J.P. Benoit, A novel phase inversion-based process for the preparation of lipid nanocarriers, Pharmaceutical Research 19 (2002) 875-880.
[23] E. Moysan, Y. González-Fernández, N. Lautram, J. Béjaud, G. Bastiat, J.P. Benoit, An innovative hydrogel of gemcitabine-loaded lipid nanocapsules: when the drug is a key player of the nanomedicine structure, Soft Matter 10(11) (2014) 1767-1777.
[24] N. Wauthoz, G. Bastiat, E. Moysan, A. Cieślak, K. Kondo, M. Zandecki, V. Moal, M.C. Rousselet, J. Hureaux, J.P. Benoit, Safe lipid nanocapsule-based gel technology to target lymph nodes and combat mediastinal metastases from an orthotopic non-small-cell lung cancer model in SCID-CB17 mice, Nanomedicine : Nanotechnology, Biology, and Medicine 11(5) (2015) 1237-1245.
[25] C. Bastiancich, K. Vanvarenberg, B. Ucakar, M. Pitorre, G. Bastiat, F. Lagarce, V. Préat, F. Danhier, Lauroyl-gemcitabine-loaded lipid nanocapsule hydrogel for the treatment of glioblastoma, Journal of Controlled Release 225 (2016) 283-293.
[26] C. Bastiancich, J. Bianco, K. Vanvarenberg, B. Ucakar, N. Joudiou, B. Gallez, G. Bastiat, F. Lagarce, V. Préat, F. Danhier, Injectable nanomedicine hydrogel for local chemotherapy of glioblastoma after surgical resection, Journal of Controlled Release 264 (2017) 45-54.
[27] C. Bastiancich, L. Lemaire, J. Bianco, F. Franconi, F. Danhier, V. Préat, G. Bastiat, F. Lagarce, Evaluation of lauroyl-gemcitabine-loaded hydrogel efficacy in glioblastoma rat models, Nanomedicine (London) 13(16) (2018) 1999-2013.
[28] Q. He, G. Su, K. Liu, F. Zhang, Y. Jiang, J. Gao, L. Liu, Z. Jiang, M. Jin, H. Xie, Sex-specific reference intervals of hematologic and biochemical analytes in Sprague-Dawley rats using the nonparametric rank percentile method, PLoS One 12(12) (2017) e0189837.
[29] Q. Wang, J. Wang, Q. Lu, M.S. Detamore, C. Berkland, Injectable PLGA based colloidal gels for zero-order dexamethasone release in cranial defects, Biomaterials 31(18) (2021) 4980-4986.
[30] Z. Gu, A.A. Aimetti, Q. Wang, T.T. Dang, Y. Zhang, O. Veiseh, H. Cheng, R.S. Langer, D.G. Anderson, Injectable Nano-Network for Glucose-Mediated Insulin Delivery, ACS Nano 7(5) (2013) 4194-4201.
[31] C. Bastiancich, E. Bozzato, U. Luyten, F. Danhier, G. Bastiat, V. Préat, Drug combination using an injectable nanomedicine hydrogel for glioblastoma treatment, International Journal of Pharmaceutics 559 (2019) 220-227.

[32] G. Bastiat, F. Plourde, A. Motulsky, A. Furtos, Y. Dumont, R. Quirion, G. Fuhrmann, J.C. Leroux, Tyrosine-based rivastigmine-loaded organogels in the treatment of Alzheimer's disease, Biomaterials 31 (2010) 6031-6038.
[33] P.Y. Li, F. Bearoff, P. Zhu, Z. Fan, Y. Zhu, M. Fan, L. Cort, T. Kambayashi, E.P. Blankenhorn, H. Cheng, PEGylation enables subcutaneously administered nanoparticles to induce antigen-specific immune tolerance, Journal of Controlled Release 331 (2021) 164-175.
[34] Y. Dölen, M. Valente, O. Tagit, E. Jäger, E.A.W. Van Dinther, N.K. van Riessen, M. Hruby, U. Gileadi, V. Cerundolo, C.G. Figdor, Nanovaccine administration route is critical to obtain pertinent iNKt cell help for robust anti-tumor T and B cell responses, Oncoimmunology 9(1) (2020) 1738813.
[35] G. Moku, S. Vangala, S.K. Gulla, V. Yakati, In vivo Targeting of DNA Vaccines to Dendritic Cells via the Mannose Receptor Induces Long-Lasting Immunity against Melanoma, Chembiochem 22(3) (2021) 523-531.
[36] M.S. Sasso, G. Lollo, M. Pitorre, S. Solito, L. Pinton, S. Valpione, G. Bastiat, S. Mandruzzato, V. Bronte, I. Marigo, J.P. Benoit, Low dose gemcitabine-loaded lipid nanocapsules target monocytic myeloid-derived suppressor cells and potentiate cancer immunotherapy, Biomaterials 96 (2016) 47-62.
[37] M. Pitorre, G. Bastiat, E. Marie dit Chatel, J.P. Benoit, Passive and specific targeting of lymph nodes: the influence of the administration route, European Journal of Nanomedicine 7(2) (2015) 121-128.
[38] C.D.V. Bessone, S.P. Akhlaghi, L.I. Tártara, D.A. Quinteros, W. Loh, D.A. Allemandi, Latanoprost-Loaded Phytantriol Cubosomes for the Treatment of Glaucoma, European Journal of Pharmaceutical Sciences 160 (2021) 105748.
[39] E. Delrish, M. Jabbarvand, F. Ghassemi, F.A. Amoli, F. Atyabi, A. Lashay, M. Soleimani, L. Aghajanpour, R. Dinarvand, Efficacy of topotecan nanoparticles for intravitreal chemotherapy of retinoblastoma, Experimental Eye Research 204 (2021) 108423.
[40] H.M. Kim, S.J. Woo, Ocular Drug Delivery to the Retina: Current Innovations and Future Perspectives, Pharmaceutics 13(1) (2021) 108.
[41] B. Grassiri, Y. Zambito, A. Bernkop-Schnürch, Strategies to prolong the residence time of drug delivery systems on ocular surface, Advances in Colloid and Interface Science 288 (2021) 102342.

[42] V.S. Kansara, M. Cooper, O. Sesenoglu-Laird, L. Muya, R. Moen, T.A. Ciulla, Suprachoroidally Delivered DNA Nanoparticles Transfect Retina and Retinal Pigment Epithelium/Choroid in Rabbits, Translational Vision Science and Technology 9(13) (2020) 21.
[43] M.C. Chang, T.Y. Luo, C.Y. Huang, C.L. Peng, K.Y. Chen, L.K. Yeh, The new ophthalmic formulation for infection control by combining collagen/gelatin/alginate biomaterial with liposomal chloramphenicol, Biomedical Physics & Engineering Express 6(4) (2020) 045017.

Graphical abstract

Polymer-free hydrogel made of lipid nanocapsules, as a local drug delivery platform.

From physico-chemistry…

… to biological evaluation.